HIGH-LIFT FLAPS FOR NATURAL LAMINAR FLOW AIRFOILS

Harry L. Morgan
NASA Langley Research Center
Hampton, Virginia 23665

SUMMARY

A review of the NACA and NASA low-drag airfoil research is presented with particular emphasis given to the development of mechanical high-lift flap systems and their application to general aviation aircraft. These flap systems include split, plain, single-slotted, and double-slotted trailing-edge flaps plus slat and Krueger leading-edge devices. The recently developed continuous variable-camber high-lift mechanism is also described. The state-of-the-art of theoretical methods for the design and analysis of multi-component airfoils in two-dimensional subsonic flow is discussed, and a detailed description of the Langley MCARF (Multi-Component Airfoil Analysis Program) computer code is presented. The results of a recent effort to design a single- and double-slotted flap system for the NASA HSNLF(1)-0213 airfoil using the MCARF code are presented to demonstrate the capabilities and limitations of the code.

INTRODUCTION

The NASA has in recent years undertaken an extensive research effort aimed at improving the aerodynamic performance of a wide range of military and civil aircraft. A large part of this research effort has been focused on improvements in cruise performance by reducing the total aircraft drag and by increasing the drag-rise Mach number of the wing. Extensive development work was performed under the leadership of NASA's Dr. Richard T. Whitcomb during the 1960's and 1970's on the NASA supercritical airfoils which have greatly improved high-speed characteristics compared to the earlier NACA 65- and 66-series airfoils developed during the 1940's wartime effort. The current NASA research effort aimed at reducing total aircraft drag involves synergetic research in the interrelated disciplines of wing aerodynamics, aircraft structures, propulsion integration, and flight control systems.

Considerable improvements in cruise performance can be achieved by reducing overall wetted-area skin-friction drag. A large percentage of the skin-friction drag associated with the high-velocity flows around the lift-producing wing and tail surfaces can be reduced by either actively or passively delaying the transition of the surface boundary layer from laminar to turbulent flow. The best active approach involves the use of distributed surface suction either through spanwise slots or porous skins. Laminar flow control (LFC) research on both forms of suction is currently being conducted in the Langley 8-Foot Transonic Pressure Tunnel. The primary objective of this research is to demonstrate the feasibility of obtaining large amounts of laminar flow on a typical moderately swept transport wing at transonic speeds and high Reynolds number.

The best passive means of controlling boundary-layer transition involves shaping the airfoil to have favorable upper and lower surface pressure gradients and carefully manufacturing the wing to eliminate surface roughness and waviness. The natural laminar flow (NLF) airfoils currently being developed at Langley (refs. 1, 2, and 3) are based on this passive means of boundary-layer control. As Mach number and Reynolds number are increased, the effects of shock-boundary-layer interaction and surface smoothness become more pronounced, and as a result, transition is more difficult to control passively. The NLF airfoils, therefore, are being designed for a subsonic Mach number range of 0.2 to 0.7 and for Reynolds numbers up to 10 million, which makes them ideally suited for application to general aviation aircraft. The greater drag reductions possible with active LFC-type airfoils are not generally applicable to general aviation aircraft because of the enormous complexity and weight penalties associated with the suction mechanisms.

In general, no matter how much effort is devoted to improving the cruise performance characteristics of an airfoil, the airfoil cannot be utilized unless it can be equipped with a flap system that will produce maximum lift coefficients great enough to prevent the necessity of unreasonable increases in wing area to meet take-off and landing performance requirements. This fact is often overlooked by airfoil designers, and as a result, many otherwise excellent airfoil designs are never put into practical use. There are very few applications for a particular airfoil that will not involve the need for some type of control surface such as flaps, slats, spoilers, and ailerons. The purpose of this paper is to present a summary of the types of flap systems that were developed for the earlier NACA low-drag and NASA supercritical airfoils and to discuss their possible application to the new NLF airfoils. The currently available theoretical methods for the analysis and design of two-dimensional flap systems will also be discussed and sample comparisons presented. Finally, the results of a recently completed effort to apply these methods to the design of a trailing-edge flap system for the HSNLF(1)-0213 airfoil will be presented and the limitations of the methods discussed.

SYMBOLS

Values are given in both SI and U.S. Customary Units. All measurements and calculations were made in U.S. Customary Units.

c airfoil chord, cm (in.)

C_p pressure coefficient, $\frac{p_\ell - p_\infty}{q_\infty}$

C_ℓ section lift coefficient

C_d section drag coefficient

C_m	section pitching-moment coefficient about quarter-chord point
M	free-stream Mach number
M_ℓ	local Mach number at a point on the airfoil
M'_ℓ	$\frac{dM_\ell}{d(s/c)}$
p	static pressure, Pa (lb/ft^2)
q	dynamic pressure, Pa (lb/ft^2)
R	Reynolds number based on free-stream conditions and airfoil chord
R_θ	Reynolds number based on local velocity and boundary-layer momentum thickness
s	distance along surface of airfoil, cm (in.)
x	airfoil abscissa, cm (in.)
z	airfoil ordinate, cm (in.)
α	geometric angle of attack, deg.
δ_f	flap deflection, deg.

Subscripts:

max	maximum
∞	free-stream conditions

Abbreviations:

F	flap
HSNLF	high speed natural laminar flow
LE	leading edge
LS	low speed
MCARF	Multi-Component Airfoil Analysis Program
MS	medium speed
NLF	natural laminar flow
SEP	separation point
TE	trailing edge

HISTORY OF NACA AND NASA LOW-DRAG AIRFOIL DEVELOPMENT

The NACA and NASA have been actively involved in the design and testing of low-drag airfoils since the early 1930's. (See reference 4.) The NACA 1-series airfoil sections were the first attempts to develop sections with prescribed pressure distributions and were the first family of NACA low-drag high-speed wing sections. The development of these first airfoils was so hampered by lack of adequate theoretical tools that they only operated well over a very small lift coefficient range. The next successive attempts were the NACA 2- to 5-series airfoil sections. These sections had relatively low maximum lift coefficients and exhibited extreme sensitivity to surface roughness. The rather large extent of laminar flow obtained on these airfoils was considered to be impractical at that time. This led to the development of the NACA 6-series airfoils which were designed for smaller extents of laminar flow and higher maximum lift coefficients. A large number of these airfoils were designed and tested due to the wartime environment of the 1940's, and many sections are still in use today. The final NACA-developed sections were those of the 7-series. These sections were designed for a greater extent of laminar flow on the lower than the upper surface, which led to lower pitching moments and higher design lift coefficients at the expense of reduced maximum lift and critical Mach number.

The NASA continued development of the low-drag airfoils beginning in the early 1970's due to the renewed interest in airfoil design as a result of the supercritical wing development work under the leadership of Langley's Dr. Richard T. Whitcomb. The low- and medium-speed (LS- and MS-series) airfoils developed during that time were intended primarily for application to general aviation and exhibited the highly aft-loaded characteristics of the supercritical sections. These sections were designed for a small extent of laminar flow on the upper and lower surfaces and for relatively high maxmimum lift coefficients, high climb lift-drag ratios, and docile stall behavior. More recently, NASA has shifted emphasis toward the NLF airfoils in an attempt to lower the cruise drag of the LS and MS airfoils, while retaining high maximum lift capability. The primary difference between these NLF airfoils and the earlier NACA 6-series airfoils is not so much in the overall design objectives but more in the theoretical methods used to design them. Today's airfoil design and analysis methods are very accurate, which means that it is no longer necessary to design and test a large number of airfoils to obtain an airfoil with the desired performance characteristics.

To date, the NASA has developed four NLF airfoils which vary in thickness, cruise lift coefficient, extent of laminar flow, and cruise Mach number. The first two of these airfoils are the NLF(1)-0416 and NLF(1)-0215F and are reported in references 1 and 2. The NLF(1)-0416 was designed for a Mach number of 0.2 with approximately 30-percent laminar flow on the upper surface and 40-percent laminar flow on the lower surface, and likewise, the NLF(1)-0215F was designed for 40-percent laminar flow on the upper surface and 60-percent on the lower surface. The third airfoil is the NLF(1)-0414F and is reported in reference 3. This airfoil was designed for a higher Mach number of 0.4 with 70-percent laminar flow

on both surfaces. The fourth airfoil is the HSNLF(1)-0213 (High-Speed NLF) which has recently undergone preliminary low- and high-speed verification tests in the Langley Low-Turbulence Pressure and 6- by 28-Inch transonic tunnels. This airfoil was designed for a cruise Mach number of 0.7 with 56-percent laminar flow on the upper surface and 67-percent on the lower surface.

Each of these four airfoils has design pressure distributions similar to that illustrated in figure 1 for the NLF(1)-0414F. The pressure gradients forward of the transition point are favorable to promote a steady growth of the laminar boundary layer and slightly adverse aft of the transition point to promote efficient transition to turbulent flow without separation. The further aft the transition point, the steeper the recovery and the more difficult it is to avoid trailing-edge separation. All of these NLF sections have less thickness and camber in the trailing-edge region than the LS and MS airfoils. These characteristics have an adverse effect on the design, and therefore, it is more difficult to design an efficient high-lift system for NLF sections. These NLF airfoils are very similar to the 6-series airfoils, but have the advantage of improved leading-edge shapes to increase maximum lift capability. When equipped with similar high-lift systems, these new NLF airfoils should perform as well, if not slightly better, than similarly equipped 6-series airfoils. The next section of this paper will present a brief review of the types of flap systems that were developed for the early NACA airfoils and the general performance characteristics associated with each.

TYPES OF MECHANICAL FLAPS

Almost all aircraft wings require some type of auxiliary device to modulate aerodynamic lift, drag, pitch, and roll in order to satisfy cruise, takeoff, and landing performance requirements. Wing sizing is perhaps the most critical item the designer of a new aircraft must consider because it directly affects wing weight, ride quality, and growth potential. Wings with poor maximum lift capability are much larger and heavier and tend to have increased friction drag which inhibits cruise performance. Since the first flight by the Wright Brothers, airfoil and high-lift system development have continued to evolve due to tremendous increases in aircraft size and cruise speeds. In recent years, a great deal of emphasis has been given to improvements in the fuel efficiency of aircraft. This emphasis has brought about a renewed interest in smaller wings producing lower drag. These smaller wings generally have high aspect ratios and operate at high cruise lift coefficients and wing loadings which require smaller, more efficient, and more complex high-lift systems to meet takeoff and landing requirements.

Smaller and more efficient wings are especially of interest to the manufacturers of military and commercial transports who are particularly concerned with the payload capability and operational costs of new aircraft. The design, manufacture, and operational maintenance difficulties associated with the more complex high-lift systems required for these wings are overshadowed by the potential benefit of increased

performance capability. In contrast, the manufacturers of the smaller general aviation aircraft are more interested in low initial costs, low maintenance requirements, and high reliability. Due to the highly competitive market for new general aviation aircraft, complex high-lift systems are not considered generally applicable. Another more desirable, although less effective, way to reduce wing drag and increase cruise performance is to reduce the skin-friction drag of the basic wing section, which has led to a renewed interest by general aviation in the development of natural laminar flow airfoils.

In general, there are four basic methods to increase the maximum lift of an airfoil: 1) increase leading- and trailing-edge camber, 2) extend the chord, 3) delay boundary layer separation, and 4) energize the external flow field. The latter two methods which encompass selective boundary layer suction and/or blowing and powered-lift concepts are extremely complex and costly to maintain and are understandably not applicable to general aviation aircraft. The discussion of high-lift systems will therefore be limited to those that utilize the first two methods.

The trailing-edge flap systems generally applicable to general aviation are presented in figure 2. The split flap is the simplest of the trailing-edge flap systems and is formed by deflecting an aft portion of the lower surface about a hinge point at the forward edge of the deflected portion. The hinge point can be located to provide a slot at the leading edge of the flap. The split flap can produce maximum C_ℓ increments in the range of 0.9 to 1.5 and possibly as high as 1.9 for very thick airfoils with large leading-edge radii. Deflecting the split flap results in a large bluff body which creates a large separation region with accompanying high drag. As an example, the performance of the several NACA 6-series and NASA NLF airfoils equipped with a 20% chord split flap is presented in figure 3 and shows average maximum C_ℓ increments of approximately 1.0.

Plain flaps are formed by hinging the trailing-edge region of the airfoil about a point within the contour and by pivoting with a downward deflection to increase the trailng-edge camber of the airfoil. This flap, like the split flap, can produce maximum C_ℓ increments in the range of 0.9 to 1.5 and are generally more effective when applied to airfoils with small amounts of camber. The drag produced by the plain flap is considerably less than that for a corresponding split flap because the upper surface is also deflected and the large bluff body with its corresponding separation is avoided. The plain flap has been used on many vintage and current production aircraft because it is easy to build, to actuate, and to maintain, and it is very reliable. As an example, the performance of the NACA 65,3-618 and NACA 66(215)-216 airfoils equipped with a 20-percent chord plain flap is presented in figure 4 and shows maximum C_ℓ increments of 0.9 and 1.0 for corresponding flap deflections of 60° and 65°, respectively. Split flaps usually produce slightly higher maximum C_ℓ increments than an equal-chord plain flap due to the loss of effective chord associated with the deflected plain flap.

The next level of trailing-edge flap system complexity is the slotted flap which is similar to the plain flap except that the flap

hinge point is located external to the airfoil and produces a slot when deflected. The slot ducts the high-energy air from the lower surface to the low-energy air on the upper surface of the downstream element to delay separation and increase flap effectiveness. The rearward motion to produce the slot also results in a chord extension which in turn increases flap effectiveness. The amount of chord extension is dependent on the cutoff point on the forward element and the deflection of the aft element. In other words, the smaller the amount of the upper surface of the flap that is exposed when nested, the greater will be the chord extension when the flap is deflected. This type of flap is extremely effective and the most widely used on existing aircraft. Many commercial transports and commuter aircraft are equipped with single-, double-, or triple-slotted flap systems. The mechanical complexity of the slotted flap varies from the simple external fixed-hinge-point arrangement, which combines rotation and translation in the same movement, to the external flap-track arrangement, which separates rotation and translation allowing for greater possible chord extension.

Although a great deal of experimental data have been accumulated over the years, a general statement concerning the maximum C_ℓ increments obtainable with slotted flaps is not possible because of the sensitivity of flap effectiveness to the number of flap elements, Reynolds number, gap and overlap settings, and element deflection. In general, however, increasing the number of flap elements tends to increase the maximum obtainable C_ℓ increments. More than two flap elements rarely provide enough additional C_ℓ to warrant the additional complexity and weight, unless the airfoil is equipped with some type of leading-edge device. An examination of the data presented in reference 3 for the NACA 6-series airfoils shows maximum C_ℓ increments in the range of 1.0 to 1.4 for single-slotted flaps and 1.4 to 1.7 for double-slotted flaps. As an example, the performance of the NACA 63_4-420 airfoil equipped with a 25-percent chord slotted flap is presented in figure 5 and shows maximum C_ℓ increments of 1.5 and 1.56 for two flap-hinge locations. Likewise, the performance of the NACA 65_3-118 airfoil equipped with a 30.9-percent chord double-slotted flap is presented in figure 6 and shows a maximum C_ℓ increment of 1.7. It is reasonable to expect the NLF airfoils, which have slightly improved leading-edge designs, to obtain maximum C_ℓ increments of 1.5 to 1.6 with a properly designed single-slotted flap and increments of 1.8 to 1.9 with a double-slotted flap.

Although not generally considered during the design of general aviation aircraft, leading-edge devices are required in order to take full advantage of the trailing-edge flap system. Four types of mechanical leading-edge devices in use on many current military and commercial aircraft are presented in figure 7. These devices are mounted ahead of the leading edge to assist in turning the flow around the leading edge, thereby, delaying flow separation to a much higher angle of attack. The complexity of these devices ranges from the rather simple drooped-leading-edge device with a single lower surface hinge point to the very sophisticated variable-camber Krueger device actuated by complex four-bar linkages. The chord of a leading-edge device nominally ranges from 10 to 20 percent of the nested chord and rarely consists of more than a single element. Like the trailing-edge flap, a slotted leading-edge device is preferred because of the beneficial ducting effect of the high-

energy lower surface air into the leading-edge boundary layer on the main element. The increment in maximum C_ℓ due to the addition of a leading-edge device is also very difficult to estimate because of the interaction of the wake from the device with the boundary layers and wakes on the downstream elements. It is not uncommon to see additional increments 30 to 40 percent greater due to the addition of a leading-edge device. As an example, the performance of an NACA 64A010 airfoil equipped with a split and a double-slotted flap and a 17-percent chord leading-edge slat is presented in figure 8 and shows incredible performance gains attributable to the slat.

As stated before, the manufacturers of general aviation aircraft have avoided the use of leading-edge devices because of the complexity and weight penalty associated with the device and because of the extensive maintenance schedule required to insure safe and reliable operation. They are not generally considered applicable to low-drag airfoils due to the adverse effects on the stability of the leading-edge laminar boundary layer resulting from surface irregularities with the device nested. These irregularities can possibly cause premature transition and a corresponding increase in trailing-edge separation with a possible loss in maximum C_ℓ capability. The Krueger leading-edge devices, which fold out from the lower surface, should not adversely affect the upper surface laminar boundary layer and possibly not the lower surface boundary layer because of the mildness of the lower-surface pressure gradient. In view of the recent advances in composite materials and de-icing mechanisms, it is reasonable to consider the use of leading-edge devices with the new NLF airfoils.

Another type of leading- and trailing-edge device, which has recently received considerable attention by transport manufacturers, is the continuous variable-camber device. These devices consist of internal shape-altering mechanisms that deflect and smoothly recontour (without steps and gaps) the leading and trailing edges of the airfoil surface. These devices can produce small deflections to optimize wing camber during climb, cruise, and descent and large deflections to provide high lift for takeoff and landing. A detailed discussion of the development of a continuous variable-camber device for application to short- and long-range commercial transports is presented in reference 5. A photograph of a working model of this concept is presented in figure 9, and details of the leading- and trailing-edge internal mechanisms are presented in figures 10 and 11, respectively. The continuous skin of the leading edge is flexed by the variable-camber mechanism to maintain a constant leading-edge radius through the entire range of deflections. In the trailing-edge region, the overall length of the upper surface skin remains constant, and an overlapping seal on the lower surface allows for articulation. These devices are particularly attractive for application to NLF airfoils because they eliminate surface discontinuities that exist with conventional high-lift devices and offer opportunity for a continuously optimized shape during the entire flight envelope.

The results of the study presented in reference 5 showed overall fuel savings as high as 4 percent utilizing variable-camber devices on existing conventional transport wings. Add to this the fuel savings

possible using NLF airfoil sections and the net fuel savings can be substantial. There are, of course, greater weight penalities associated with continuous variable-camber devices compared to the other less complex high-lift systems. However, recent advances in composite materials technology are making this type of high-lift device more feasible, at least for application to transport aircraft. Variable-camber trailing-edge devices do not generally produce maximum C_ℓ increments as great as those of conventional slotted-flap devices because there are no slots to duct high-energy air from the lower surface of the main wing to the upper surface of the flap. The variable-camber mechanism can be modified to create a single- or double-slotted flap by allowing several linkage pivot-points to be located external to the airfoil contour as illustrated in figure 12. This double-slotted flap mechanism also allows for positive deflections which will allow the pilot to continuously alter the wing shape to optimize cruise performance.

As previously mentioned, it is very difficult to empirically formulate performance estimates for slotted-flap systems because of their sensitivity to Reynolds number and position. There are, however, theoretical methods and corresponding computer codes that attempt to model the complex flow around high-lift flaps and provide the designer with valuable tools to estimate performance. The next section of this paper will discuss some currently available and widely used methods to analyze high-lift flap systems.

THEORETICAL DESIGN AND ANALYSIS METHODS

The flow field around an airfoil with a deflected slotted leading- and trailing-edge flap system is very complex as illustrated in figure 13. Ordinary laminar and turbulent boundary layers and downstream wakes exist on each element. For optimum performance, the elements must be located in close proximity to one another which results in the interaction of the downstream wake of the forward elements with the boundary layers on the downstream elements. These interacting merged flows are called confluent boundary layers. Usually, at or near the maximum C_ℓ conditions, one or more regions of separated, highly rotational flow exist. The cove geometric discontinuities associated with the main-element flap cutout also create local separation and reattachment regions.

Both linear and nonlinear methods have been used to model the complex flow field around slotted flap systems. The nonlinear methods which directly couple viscid and inviscid flow regions involve the use of finite-element or finite-difference numerical techniques to solve some form of the time-dependent Navier-Stokes equations. These nonlinear methods require rather dense field grid networks to adequately represent the viscous effects, which in turn require rather large computer capacity for solution. Although excellent progress has been made applying these methods to the analysis of unflapped airfoils and wings, very little progress has been made applying them to the flapped configurations. Computer capacity and execution speeds are increasing at a phenomenal rate, and hopefully, complete nonlinear solutions will be possible within

the next decade. Even then, this type of solution method will probably not be used on a routine basis for some further period of time because of the large computation time and high costs involved. A more logical application would be to use linear methods to improve the models used in the nonlinear methods.

The linear methods assume that, although the shear forces are interrelated with the pressure forces through the boundary layer, the viscid and inviscid regions can be solved separately and then iteratively interacted with each other. One such method that uses this solution philosophy is the NASA-developed Multi-Component Airfoil Analysis computer code (MCARF) which was the product of a joint effort with NASA, Lockheed-Georgia Company, and Boeing Commercial Airplane Company and is documented in references 6 and 7. The current version of this program is only applicable to flapped airfoils with smooth geometry and no separated flow regions in subsonic flow. The Laplace equation is used to solve the inviscid potential flow which is assumed to be irrotational. Utilizing the Biot-Savart law, the airfoil components are represented by a series of connected constant or linearly varying vortex and source singularities whose strengths are determined using matrix inversion techniques. The viscous displacement effects due to the wake and surface boundary layers are computed using integral techniques to solve the ordinary and confluent boundary layer equations. During successive iterations, the viscous displacement effects are accounted for by either decambering the airfoil shape or by imposing an additional source distribution whose strength is proportional to the rate of change of the boundary-layer displacement thickness. The current version of MCARF uses the decambering technique because it requires less computational time and provides an answer approximately 90-percent that obtained using the distributed source technique. It is believed, however, that use of the distributed source technique will be necessary to properly simulate massive separation regions. The output from the MCARF computer code consists of surface pressure and velocity distributions, boundary-layer properties, and integrated force and moment coefficients. An auxiliary computer code called TRACE is available to map streamline patterns around a multi-component airfoil and uses the vortex and source strengths computed by MCARF as input. Work is currently underway on a version of MCARF which can account for fixed external boundaries such as wind-tunnel floors and ceilings. Preliminary results from this improved version are presented in figure 14 showing the streamline pattern for a typical single-slotted flap with simulated floor and ceiling boundaries corresponding to that for the Langley Low-Turbulence Pressure Tunnel (LTPT).

Although the current version of the MCARF code does not contain a separated flow model, the code can be used to predict the maximum C_ℓ of airfoils with leading-edge stall properties which are characteristic of many supercritical and NLF airfoils. Leading-edge stall occurs when the angle of attack is great enough to induce sufficient instability of the laminar boundary layer to prevent transition to a reattached turbulent boundary layer. At lower angles of attack, the reattached turbulent boundary layer will remain attached to the trailing edge of the airfoil. At the stall angle, the laminar boundary layer separates and a massive separation region forms resulting in a dramatic loss in C_ℓ. The

integral laminar boundary layer method of Cohen-Reshotko (ref. 8) transformed for compressible flow by Stewartson's transformation (ref. 9) is used in the MCARF program to compute the laminar boundary-layer properties. The Schlichting-Ulrich-Granville method (refs. 10 and 11) is used to predict the point of laminar instability and subsequent point of transition.

To date, no exact method exists to determine whether the laminar boundary layer will remain completely separate or reattach as a turbulent boundary layer. The Goradia-Lyman laminar stall criterion (ref. 12) suggests that a pair of nondimensional parameters based on the Mach number, Mach number gradient, and momentum Reynolds number at the separation point can be used to predict the existence of turbulent reattachment. Extensive correlations between available experimental data and theory predictions have generally shown poor agreement using the pair of parameters proposed by Goradia-Lyman. Better agreement has been obtained by formulating the following modified pair of parameters which also incorporates the influence of free-stream Mach number and Reynolds number:

$$\left(\frac{R_\theta}{\sqrt{R/10^6 - R_\theta/10^3}} \right)^{1/2} \tag{1}$$

$$\frac{-M_\ell'}{\sqrt{M_\ell - M}} \tag{2}$$

Figure 15 shows a curve for predicting laminar stall based on the theoretical predictions from the MCARF code. The primary data used to develop this laminar separation curve included experimental-theory correlations for the NACA 0012, NACA 23012, NACA 65_2-215, and the NASA NLF(1)-0416 airfoils.

Additional experiment-theory correlations have been performed to determine the validity of using the laminar separation curve to predict laminar stall and corresponding maximum C_ℓ for flapped airfoils. The most comprehensive data available on a laminar-stall-type airfoil equipped with a wide variety of the leading- and trailing-edge high-lift devices are those for the 9.3-percent-thick supercritical airfoil reported in reference 13. Figure 16 shows the theory-experiment comparison for the basic unflapped section. Lift, drag, and pitching-moment agreement is good until the turbulent boundary layer begins to separate near the trailing edge. Although the separation method predicts the correct maximum C_ℓ, the predicted stall angle is approximately 2° less than the experimental value. However, the separation method is not expected to perform as well for unflapped airfoils that may have rather large regions of trailing-edge separation at maximum C_ℓ, which is typical of many of the NASA-developed low- and medium-speed general aviation airfoils or the recently developed NLF(1)-414 and HSNLF(1)-0213 airfoils.

Presented in figures 17 and 18 are theory-experiment comparisons for the supercritical airfoil equipped with a single-slotted flap deflected 20° and 30°, respectively. The agreement with the flap deflected 20° is excellent. Although the overall agreement for C_ℓ is poor with the flap deflected 30°, the predicted maximum C_ℓ agrees well with the experimental value. An examination of the experimental flap pressure distributions for the 30° case shows that the flow is separated on approximately 10% of the upper surface near the trailing edge which accounts for the poor agreement between experiment and theory. It should not be generally concluded, however, that the code will predict the correct maximum C_ℓ with flap separation present. Without proper modelling of the separation region on the flap, the predicted flap loads are too high and produce a greater circulation around the main element and more adverse pressure gradient in the leading-edge region than occurs experimentally. The code will, therefore, predict a lower stall angle than that obtained experimentally. In order to incorporate a separation model in the MCARF code for flapped airfoils, a criterion for the accurate prediction of the separation point for merging confluent boundary layers is needed. To date, no such criterion has been developed; therefore, only ordinary turbulent boundary layer methods can be used to indicate possible flow separation.

The theory-experiment comparison for the supercritical airfoil equipped with a leading-edge device is presented in figure 19 and shows good agreement for lift and pitching moment. Maximum C_ℓ prediction is based on laminar boundary layer separation on the leading-edge device and shows good agreement, even though the experimental data show separation present near the trailing edge of the main element. The rather poor drag agreement can be attributed to errors in the downstream wake measurements caused by flow disturbances from the support brackets for the leading-edge device. The theory-experiment comparisons for the airfoil equipped with a triple-slotted trailing-edge flap and no leading-edge device and with a double-slotted trailing-edge flap and leading-edge slat are presented in figures 20 and 21, respectively. The agreement is good for both flapped airfoils shown, and again, the maximum C_ℓ in each case is based on the laminar stall of the most forward element. The two flap configurations shown are at relatively low deflections and the flow is attached on all flap elements. Additional correlations have shown that the prediction accuracy of the MCARF code deteriorates rapidly with increased flap deflection and accompanying flap separation.

FLAP SYSTEM FOR HSNLF(1)-0213 AIRFOIL

A large percentage of the experimental tests conducted by the NACA during the development of flap systems for the 6-series airfoils were performed in the Langley LTPT facility. This unique two-dimensional test facility can obtain a maximum Mach number of approximately 0.45 and a maximum Reynolds number of approximately 18 million per foot. The LTPT has recently undergone extensive renovation to improve the facility's operating characteristics. (See reference 14.) A new model-support and force-balance system and a sidewall boundary-layer control system were included in the renovation to improve the high-lift testing capability of

the tunnel. The cooling coils were replaced to extend the cold weather operating pressures of the facility and the antiturbulence screens replaced to reduce the free-stream turbulence of the flow. As a result of these modifications, the LTPT facility is now considered to be one of the best tunnels in existence for the development of low- and medium-speed NLF airfoils and low-speed high-lift flap systems.

Due to the unique operational characteristics of the LTPT, the facility is in heavy demand by government and non-government organizations conducting research on a wide range of laminar flow and high-lift-related topics. The Langley 6- by 28-Inch Transonic Tunnel, which is a blowdown facility and uses the LTPT as a primary high-pressure air-storage tank, is also in heavy demand by researchers developing high-speed and transonic airfoils. Due to the heavy demand on both facilities and due to a limitation on the number of operating personnel, the test time available for any given experiment is rather limited and the test objectives very selective. Tunnel time is no longer readily available to conduct tests on large families of airfoils or high-lift systems; therefore, design and analysis methods are used extensively to reduce the development time. In fact, in many instances the primary objective of a typical test scheduled for the LTPT and the 6- by 28-Inch Transonic Tunnel is to either verify a particular theoretically designed airfoil system or to provide data needed to improve the design and analysis methods. The remaining discussion in this paper will describe one such research effort and involves the design of a trailing-edge flap system for the recently developed HSNLF(1)-0213 airfoil. The single- and double-slotted flap systems designed for this airfoil have not been experimentally verified to date.

The structural wing box for most high-speed general-aviation and transport aircraft has a length which is nominally 50 percent of the local wing chord and is positioned with 20 percent of the chord forward of the wing box available for leading-edge devices and 30 percent aft available for trailing-edge devices. For the HSNLF(1)-0213, an additional 2 percent immediately aft of the wing box was allowed for structural interface with a flap actuation system which resulted in a nested trailing-edge flap chord length of 28 percent of the total wing chord. The recessed cove region formed in the lower surface trailing edge of the main element when the flap is deflected produces a local separation bubble with a reattachment point at the exit of the slot between the main and flap elements. It is desirable to locate the cutoff point as far forward as possible on the lower surface of the main element to insure smooth pressure recovery through the slot region. The lower surface geometry of the single-slotted flap design is, therefore, the same as that of the aft 26 percent of the lower surface of the basic section. The bulk of the flap design effort is therefore centered around contouring the upper surface of the flap. After selecting the upper surface cutoff point for the main element, the flap design contour is further limited to that enclosed within the flap cove region of the main element.

The flap contours for the HSNLF(1)-0213 airfoil that result from selecting upper main element cutoff points at 88, 92, 96, and 98 percent of the total chord are presented in figure 22. The advantage of moving

the cutoff point further aft toward the trailing edge is an increase in the effective chord with the flap extended which should produce a corresponding incremental increase in C_ℓ. The primary disadvantage to moving the cutoff further aft is that, in order to obtain an acceptable structural thickness in the trailing-edge region of the main element, the maximum thickness and leading-edge camber of the flap must decrease, which will result in a possible incremental decrease in C_ℓ. The performance of each of the four flap designs was determined using the MCARF computer code for flap deflections of 35° and 40° with a 2-percent gap and a 0-percent overlap at a Mach number of 0.1 and a Reynolds number of 4 million. The stall angle for each case was assumed to occur at the angle corresponding to separation of the laminar boundary layer at the upper surface transition point. A check for flap separation was made by performing an ordinary turbulent boundary layer analysis of the upper surface flap pressure distribution for all four cutoff designs at the same flap deflection. It was assumed for comparison purposes that the more forward the predicted separation point, the greater the loss in the maximum C_ℓ. Until a separation model can be formulated and incorporated into the MCARF computer code, only empirical estimates can be made of the exact loss in maximum C_ℓ due to flap separation. No attempt was made during this design effort to determine an empirical correlation; therefore, the maximum C_ℓ values presented are probably higher than those which could be obtained experimentally.

A comparison of the lift and drag performance predictions for the 88- and 92-percent flap designs is presented in figure 23 for flap deflections of 35° and 40°. At a given angle of attack, the C_ℓ for the 92-percent flap design was approximately 0.1 higher than that for the 88-percent design and the corresponding increment in maximum C_ℓ was approximately the same. Examination of the lift-drag polars shows slightly higher drag for the 92-percent design with 35° flap deflection and very little difference at 40° deflection. These results indicate a slight performance advantage of the 92-percent flap design over the 88-percent flap design. A comparison of the corresponding lift and drag performance predictions for the 92- and 96-percent and the 92- and 98-percent flap designs are presented in figures 24 and 25, respectively. Both comparisons show a negligible increase in maximum C_ℓ at 35° deflection and an approximate 0.2 increase at 40° deflection. The drag polars, however, show a variation in the increase in drag coefficient of 25 percent at low C_ℓ values to approximately 5 percent near maximum C_ℓ. A turbulent boundary-layer analysis of the flap pressure distributions of each flap design at 35° deflection indicated that approximately 31, 21, and 17 percent of the upper surface was separated for the 88-, 96-, and 98-percent designs as compared to 14 percent for the 92-percent design. A comparison of the geometries and of the flap pressure distributions for the four designs at an angle of attack of 0° and a flap deflection of 35° is presented in figure 26. The comparison of the flap geometries shows a forward movement of the maximum thickness location as the cutoff point is moved further aft, which results in higher overall velocities in the slot region and reduced flap separation. The 92-percent flap is proportionally thicker aft of the maximum thickness point compared to the others, which reduces the upper surface pressure recovery and further decreases flap separation.

The results of the analysis of the performance predictions for the four flap designs indicate a slight advantage of the 92-percent design over the other three. The reduction in flap thickness that occurred by moving the cutoff location from 88 to 92 percent results in a slight structural disadvantage for the flap element but not for its corresponding main element which is thicker in the trailing-edge region. The 92-percent design is, therefore, recommended for application with the HSNLF(1)-0213 airfoil.

The next phase of the design effort was the design of a double-slotted flap with the same 28-percent nested chord length. The vane (forward flap element) had to be concealed in the cove region of the main element which meant that its geometry was completely arbitrary. The design of the aft flap had the same type of constraints as that for the single-slotted flap design. It was decided to design the vane-flap combination so that the vane remained in a fixed position relative to the aft flap element as the flap combination deflects. The simplest type of actuation system is a fixed external-hinge mechanism. The 88-percent single-slotted flap was selected as the starting geometry. After many hours of trial-and-error vane and flap contouring, the geometries presented in figure 27 were finalized. The vane element has a chord of approximately 8 percent and the aft flap element a chord of 20.5 percent. The upper surface cutoff point for the main element had to be moved forward to 87 percent to allow for the passage of the vane element through the cove opening for flap deflections greater than 20°. At a deflection of 20°, the lower surface of the vane forms a smooth contour between the upper- and lower-surface cutoff points on the main element. For flap deflections greater than 25°, the lower-surface trailing-edge deflector can be deflected upward into the cove approximately 15° to provide for a smoother cove region which should improve the acceleration of the flow through the slot and the pressure recovery on the upper surface of the vane and aft-flap elements.

The primary advantage of the double-slotted flap over the single-slotted flap is that the second slot allows for additional energization of the flap boundary layer which should delay separation and increase flap effectiveness. In other words, the vane performs the same function for the aft-flap as a leading-edge device would for the main element. A sample predicted C_p distribution for the double-slotted flap at 55° deflection is presented in figure 28. An analysis of the predicted performance data showed a very small increase in the load on the aft-flap element with an increase in deflection greater than 35°. The load on the vane element, on the other hand, increased substantially for deflections greater than 25° and reached unrealistic suction C_p values of -11 at 60° flap deflection. It is doubtful that the flow on the vane will remain attached at deflections greater than approximately 55°. A prediction of the maximum C_ℓ based on output from the MCARF computer code for the double-slotted flap through a range of deflections from 20° to 65° and for the single-slotted flap at deflections of 35° and 40° is presented in figure 29. Both the double-slotted flap at 55° deflection and the single-slotted flap at 40° deflection have the same maximum C_ℓ of approximately 3.7. An analysis of the turbulent boundary layer for the double- and single-slotted flaps at this equivalent condition showed

no separation on the vane and aft-flap of the double-slotted flap and approximately 30-percent upper-surface separation for the single-slotted flap. This indicates that the double-slotted flap is a much more effective flap than the single-slotted flap and should be used for applications requiring relatively high maximum wing lift. Another factor which should be considered before selecting the double- over the single-slotted flap is that the double-slotted flap will be heavier and more difficult to actuate than the single-slotted flap.

The effects of Reynolds number on the maximum C_ℓ of the double-slotted flap at 55° deflection and the single-slotted flap at 40° deflection are presented in figure 30. The maximum C_ℓ values presented were based on separation of the leading-edge laminar boundary layer on the main element and do not include corrections for the effects of trailing-edge flap separation. As shown in figure 30, the Reynolds number effect on both flap designs is very large with a substantial loss in maximum C_ℓ occurring at Reynolds number less than 4 million. This type of trend is common for NLF airfoil sections due to the relative sensitivity of the stability and separation of the leading-edge laminar boundary layer to a reduction in Reynolds number. This trend was also noted during the NACA tests of a 64_1A212 airfoil equipped with a leading-edge slat and a double-slotted flap as reported in reference 15. A summary of the maximum C_ℓ values obtained as a function of Reynolds number for this particular airfoil is presented in figure 31 and show trends similar to those noted for the HSNLF(1)-0213 airfoil.

CONCLUDING REMARKS

The theoretical methods available for the design and analysis of multi-component airfoils are readily available and are generally easy to use. The linearized singularity-type methods do not model the flow as accurately as the nonlinear finite-difference-type methods, but they are less costly to execute and are better suited to preliminary design and analysis tasks. Most of the currently available linearized methods do not contain separation models, which prevents reliable maximum lift predictions for airfoils and flaps with trailing-edge separation. Although several separation models are available, they cannot be used until reliable methods are developed for the prediction of the separation point for both turbulent and confluent boundary layers. The development of these methods will require the acquisition of detailed experimental data on separating boundary layers which is now possible due to the advances in the non-intrusive laser velocimetry instrumentation.

The recently completed task to design a flap system for the HSNLF airfoil demonstrated the usefulness of these theoretical methods. The selection of either the single- or double-slotted flap is dependent on the particular aircraft performance requirements. The double-slotted flap is better suited to aircraft which require low approach speeds or have relatively high wing loadings. The single-slotted flap, which will produce less maximum C_ℓ, is better suited to aircraft with low wing loadings and higher approach speeds. The theoretical analysis methods cannot reliably predict the exact maximum C_ℓ; therefore, experimental

tests need to be conducted prior to the selection of either flap system. High-lift airfoil models are considerably more complex and expensive to build than conventional airfoils and should only be tested in facilities with adequate tunnel sidewall boundary-layer treatment in order to obtain the correct performance characteristics, especially near stall.

REFERENCES

1. Somers, Dan M.: Design and Experimental Results for a Flapped Natural-Laminar-Flow Airfoil for General Aviation Applications. NASA TP-1865, 1981.

2. Somers, Dan M.: Design and Experimental Results for a Natural-Laminar-Flow Airfoil for General Aviation Applications. NASA TP-1861, 1981.

3. McGhee, Robert J.; Viken, Jeffrey K.; Pfenninger, Werner; Beasley William D.; and Harvey, William D.: Experimental Results for a Flapped Natural-Laminar-Flow Airfoil with High Lift/Drag Ratio. NASA TM-85788, 1984.

4. Abbott, Ira H.; and Von Doenhoff, Albert E.: Theory of Wing Sections. Dover Publications, New York, 1959.

5. Preliminary Design Department of the Boeing Commercial Airplane Company: Assessment of Variable Camber for Application to Transport Aircraft. NASA CR-158930, 1980.

6. Stevens, W. A.; Goradia, S. H.; and Braden, J. A.: Mathematical Model for Two-Dimensional Multi-Component Airfoils in Viscous Flow. NASA CR-1843, 1971.

7. Brune, G. W.; and Manke, J. W.: An Improved Version of the NASA-Lockheed Multielement Airfoil Analysis Computer Program. NASA CR-145323, 1978.

8. Cohen, Clarence B.; and Reshotko, Eli: The Compressible Laminar Boundary Layer with Heat Transfer and Arbitrary Pressure Gradient. NACA TR-1294, 1956.

9. Stewartson, K.: Correlated Incompressible and Compressible Boundary Layers. Proc. Roy. Soc. (London), Ser. A, Vol. 200, No. 1060, Dec. 22, 1949, pp. 84-100.

10. Schlichting, H.; and Ulrich A.: Zur Berechnung des Umschlages Laminar-Turbulent. Jahrbuch d. dt. Luftfahrtforschung, No. 1, 1942, pp. 8-35.

11. Granville, Paul S.: The Calculation of the Viscous Drag of Bodies of Revolution. Rep. 849, David Taylor Model Basin, July 1953.

12. Goradia, Suresh H.; and Lyman, Victor: Laminar Stall Prediction and Estimation of Maximum Lift Coefficient. Journal of Aircraft, Vol. 11, No. 9, Sept. 1974, pp. 528-536.

13. Omar, Z.; Zierten, T.; Hahn, M.; Szpiro, E.; and Mahal, A.: Two-Dimensional Wind-Tunnel Tests of a NASA Supercritical Airfoil with Various High-Lift Systems. Volume II - Test Data. NASA CR-2215, 1977.

14. McGhee, Robert J.; Beasley, William D.; and Foster, Jean M.: Recent Modifications and Calibration of the Langley Low-Turbulence Pressure Tunnel. NASA TP-2328, 1984.

15. Quinn, John H., Jr.: Tests of the NACA 64_1-A212 Airfoil Section with a Slat, A Double Slotted Flap, and Boundary Layer Control by Suction. NACA TN 1293, 1947.

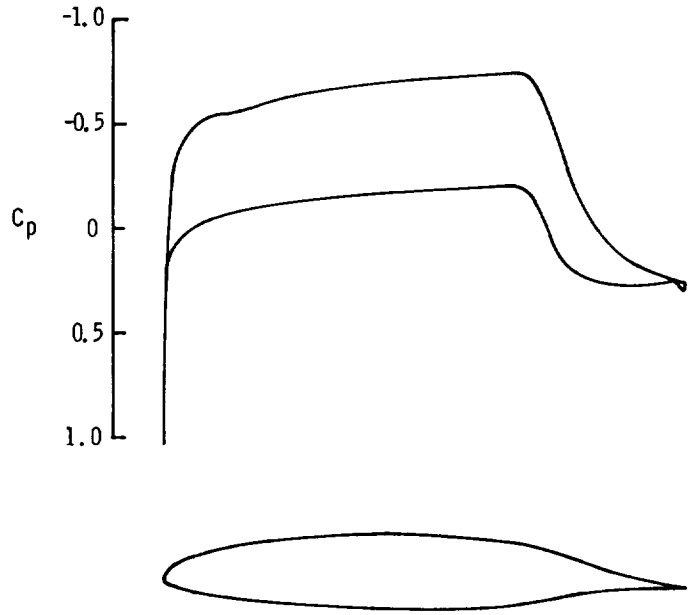

Figure 1.- Calculated pressure distribution for NLF(1)-0414F airfoil at design conditions. (C_ℓ = 0.43, M = 0.40, R = 10 × 10^6)

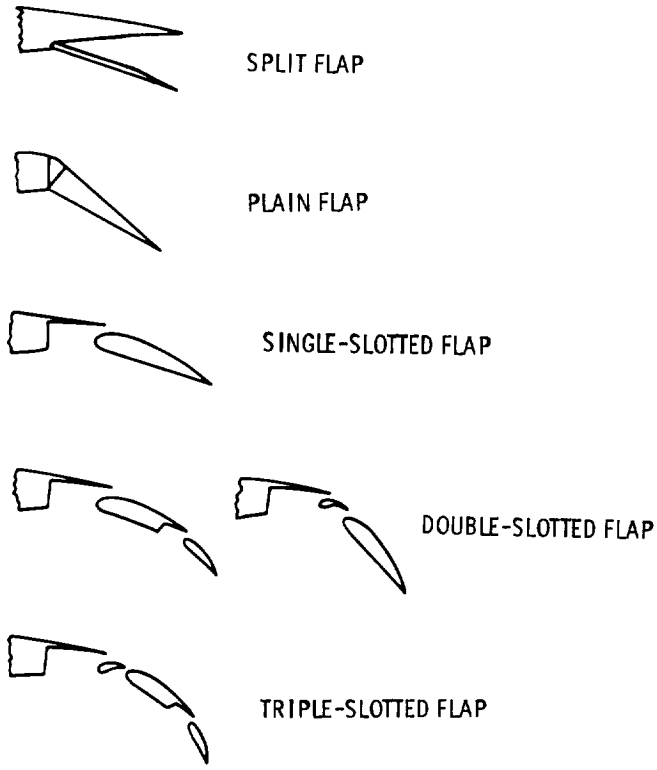

Figure 2.- Mechanical high-lift trailing-edge devices.

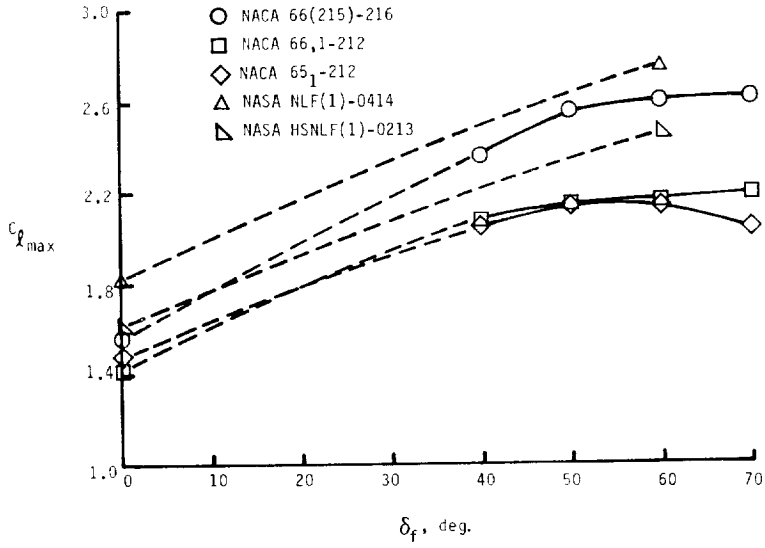

Figure 3.- Maximum lift coefficients for several NACA and NASA airfoils equipped with 0.20-chord split flaps. ($R = 6 \times 10^6$)

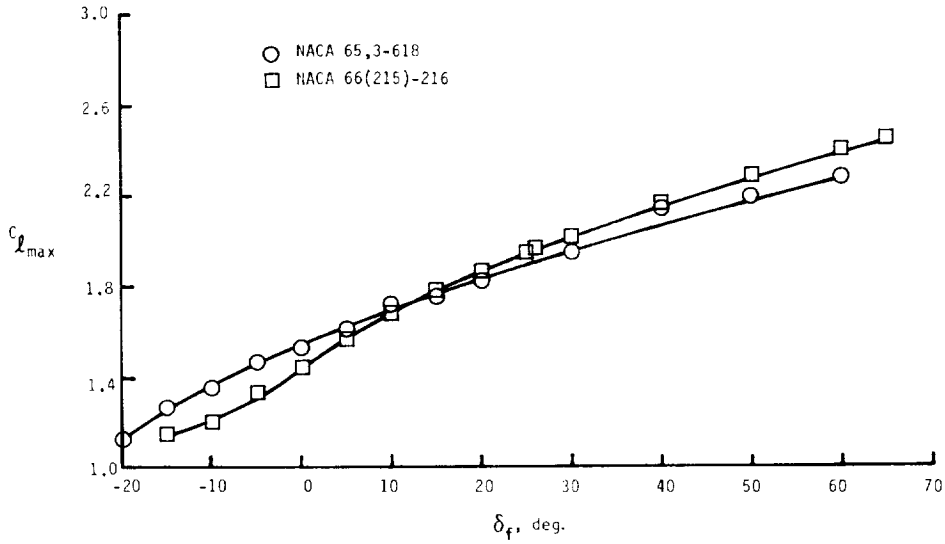

Figure 4.- Maximum lift coefficients for two NACA airfoils equipped with 0.20-chord plain flaps. ($R = 6 \times 10^6$)

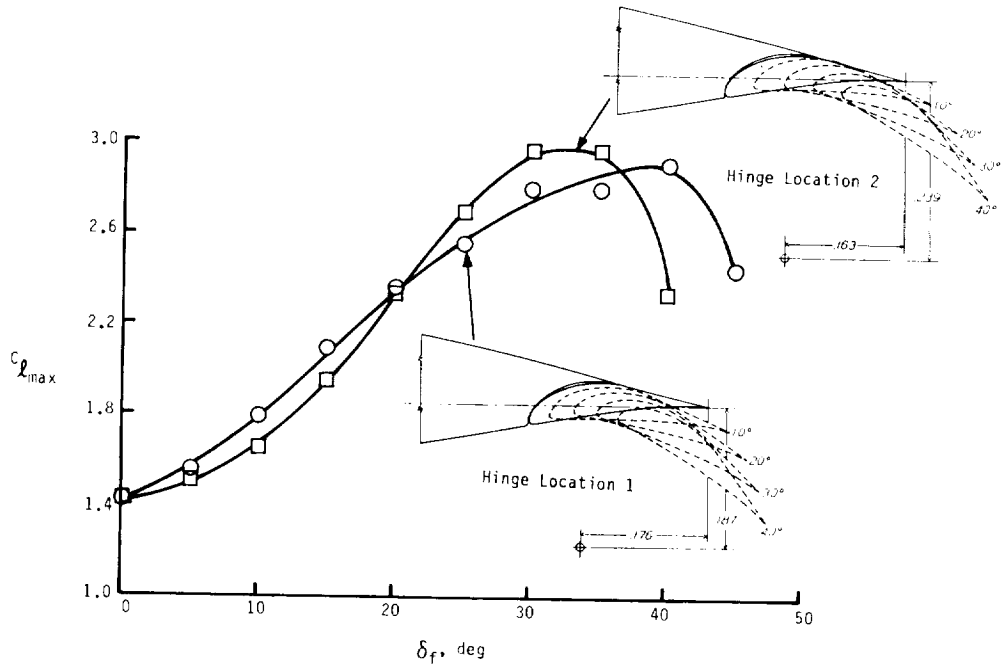

Figure 5.- Maximum lift coefficients for the NACA 63_4-420 airfoil equipped with 0.25-chord single-slotted flap. ($R = 6 \times 10^6$)

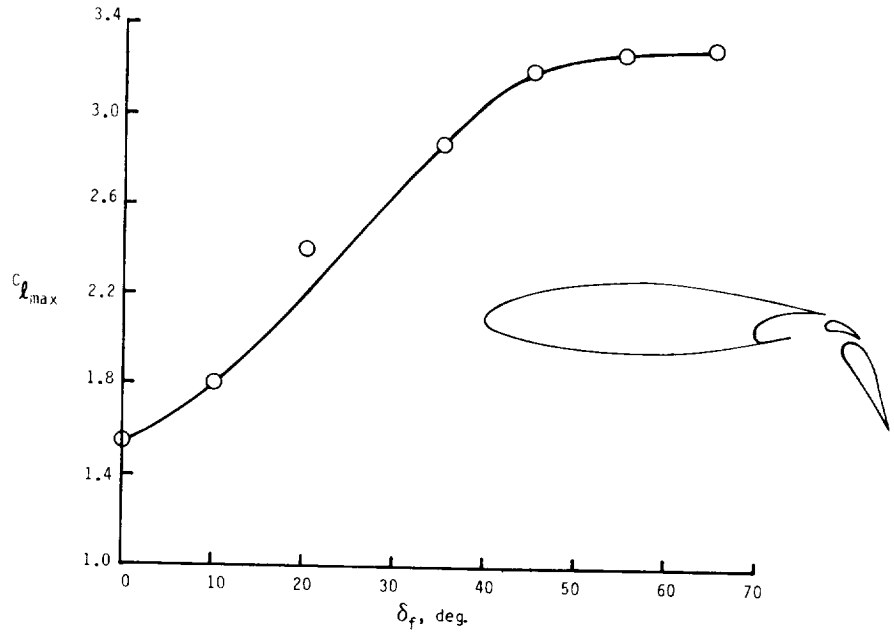

Figure 6.- Maximum lift coefficients for NACA 65_3-118 airfoil equipped with double-slotted flap. ($R = 6 \times 10^6$)

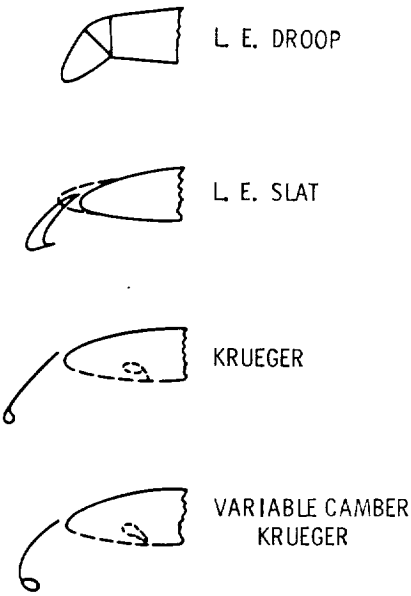

Figure 7.- Mechanical high-lift leading-edge devices.

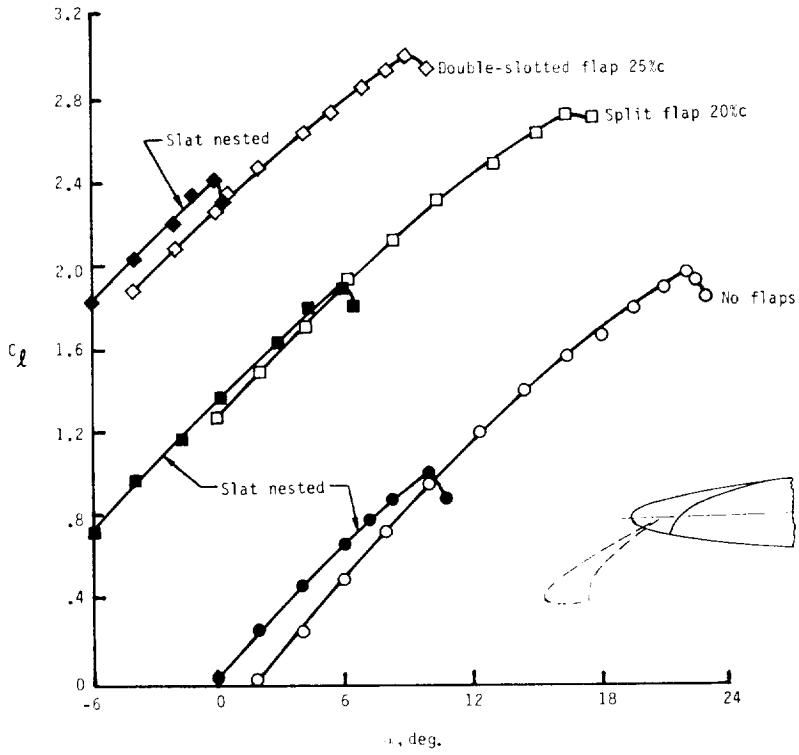

Figure 8.- Effect of leading-edge slat on performance of NACA 64A010 airfoil with and without flaps. ($R = 6 \times 10^6$)

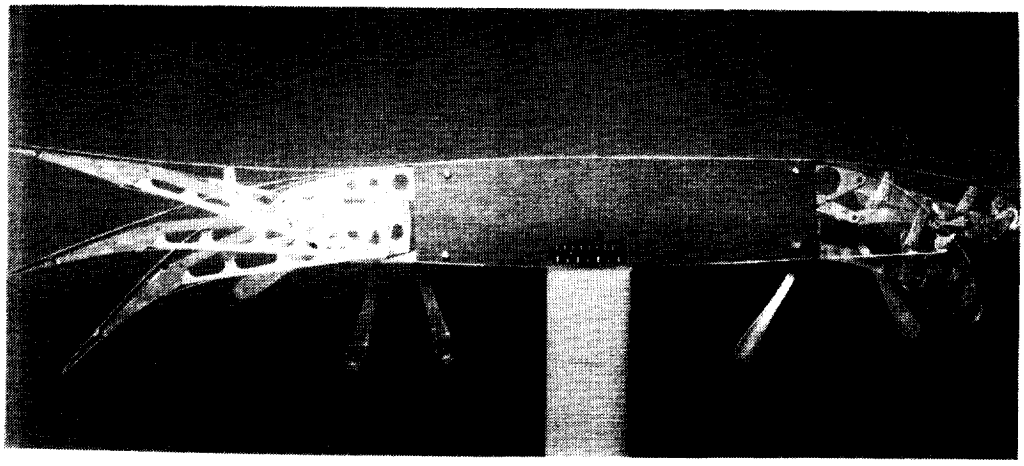

Figure 9.- Photograph of variable-camber high-lift mechanism.

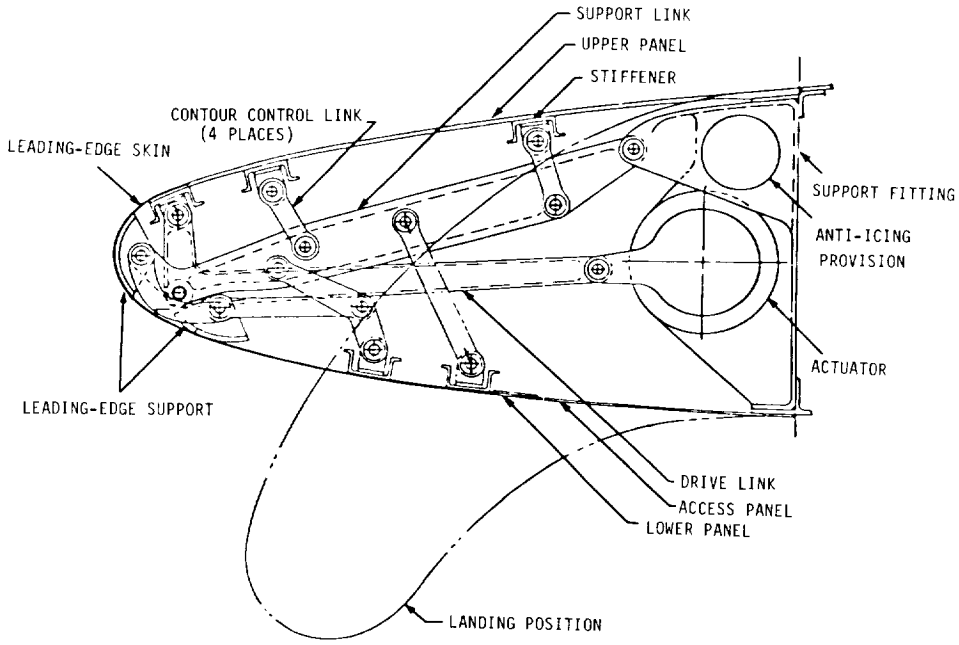

Figure 10.- Sketch of variable-camber leading-edge device.

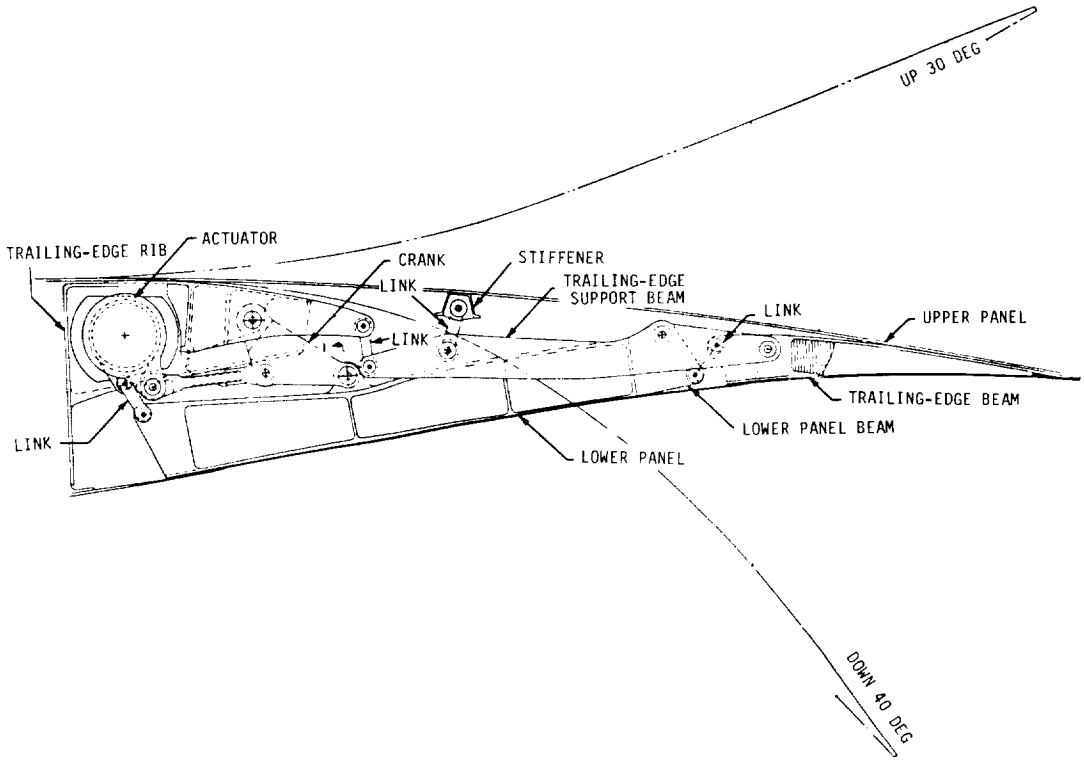

Figure 11.- Sketch of variable-camber trailing-edge device.

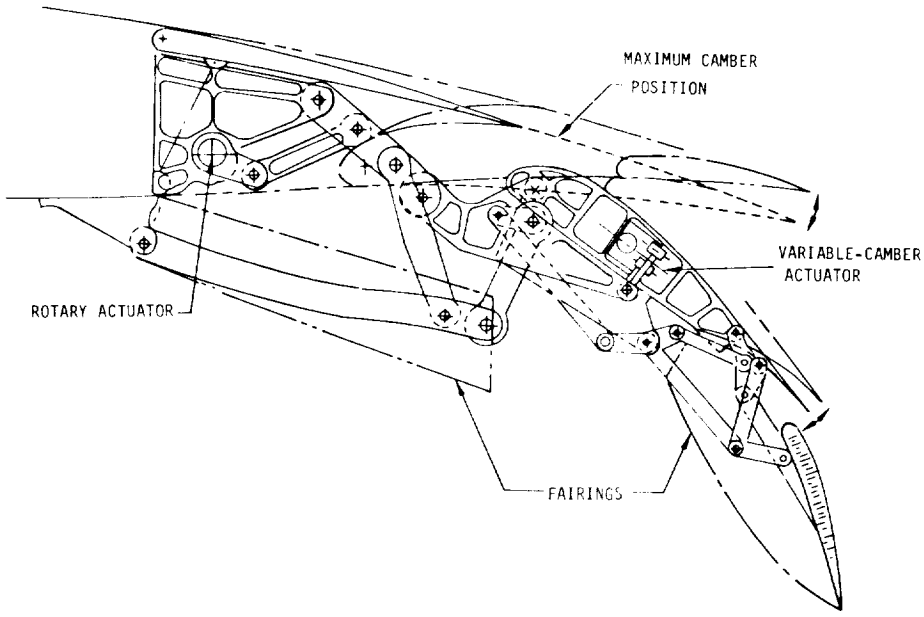

Figure 12.- Sketch of double-slotted, variable-camber trailing-edge device.

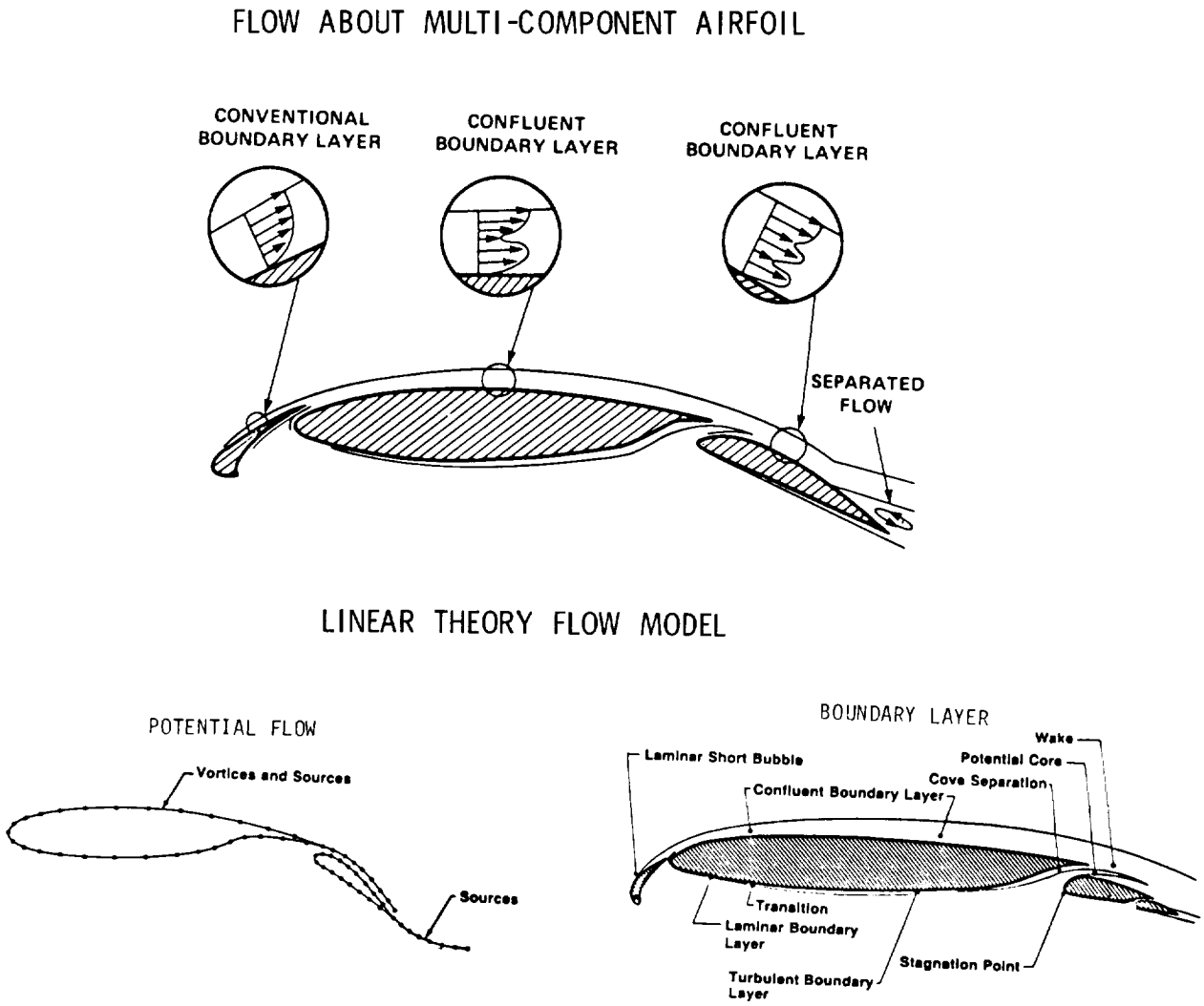

Figure 13.- Flow field and theoretical model for multi-component airfoils.

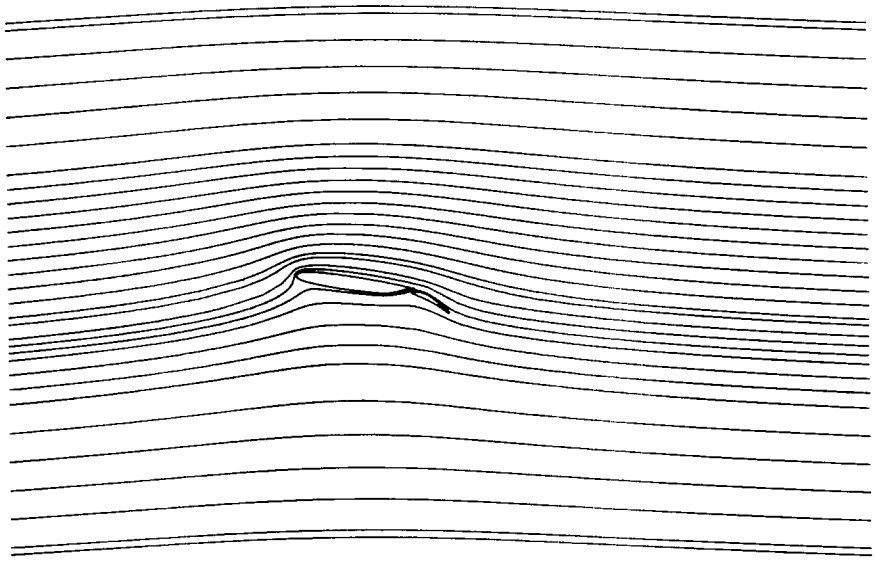

(a) Without floor and ceiling.

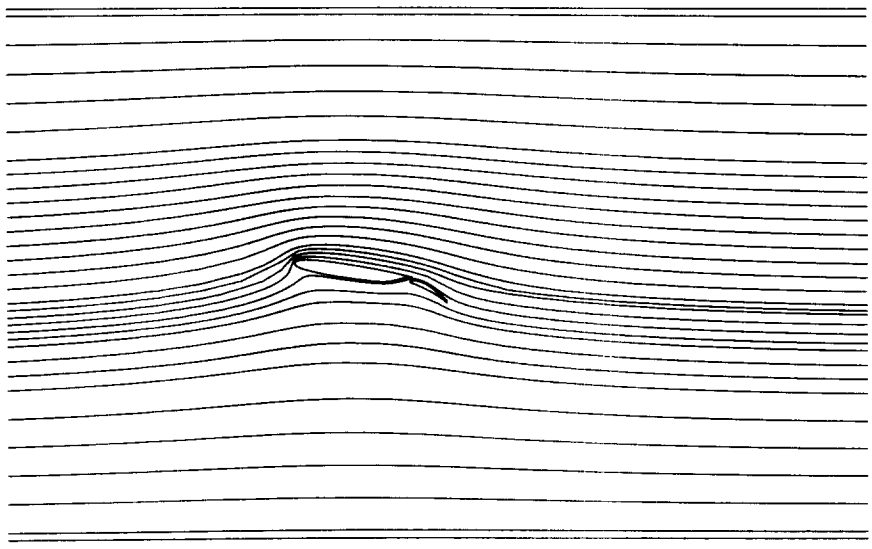

(b) With floor and ceiling.

Figure 14.- Streamline trace for typical single-slotted flap with and without floor and ceiling simulation.

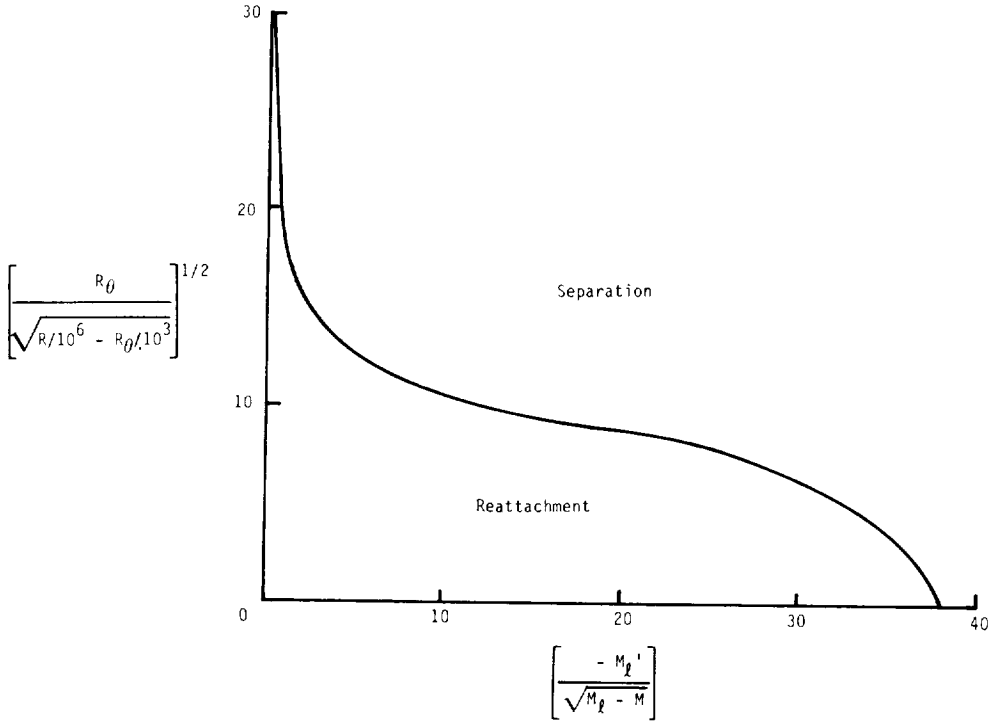

Figure 15.- Laminar boundary layer separation-reattachment curve.

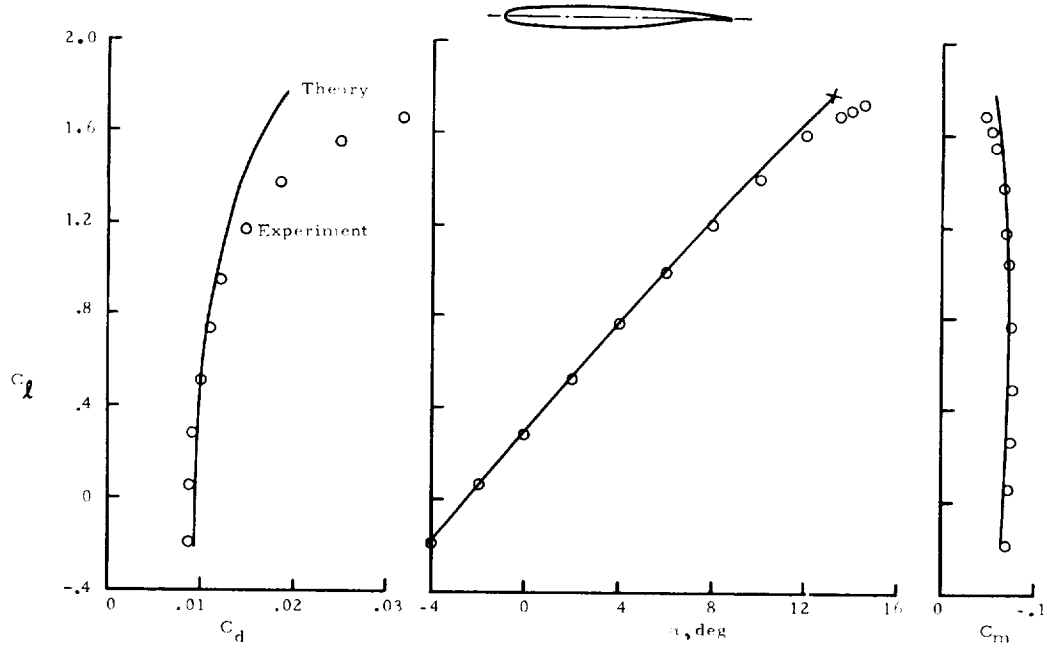

Figure 16.- Theory-experiment comparison for 9.3% thick supercritical airfoil.

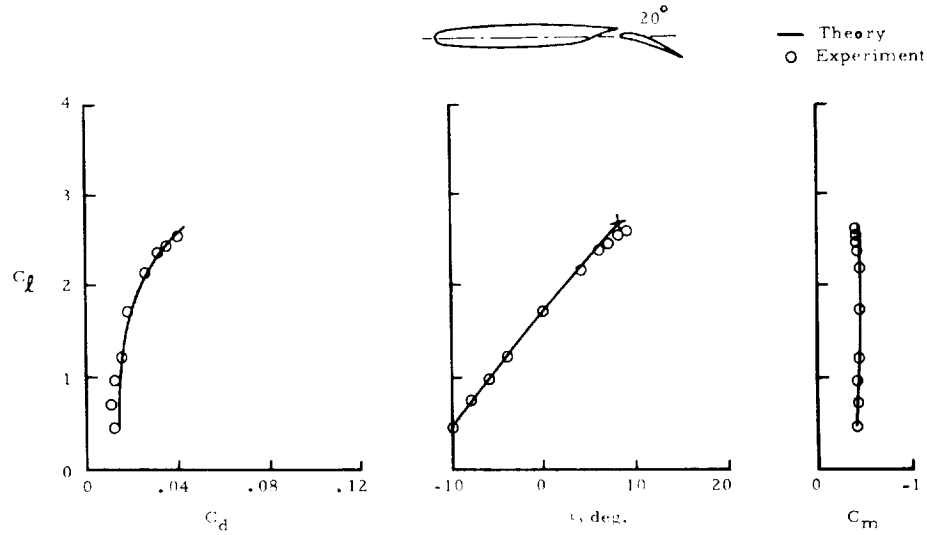

Figure 17.- Theory-experiment comparison for 9.3% thick supercritical airfoil equipped with a single-slotted flap at 20° deflection.

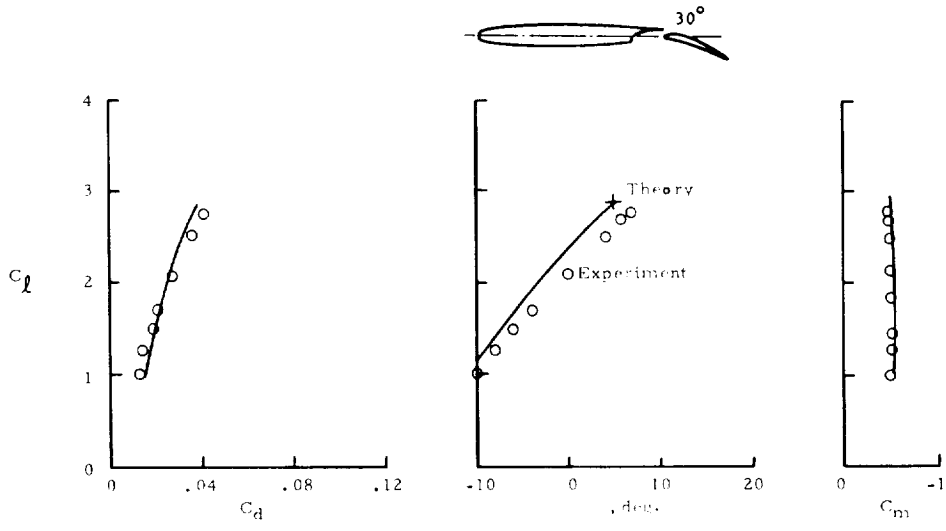

Figure 18.- Theory-experiment comparison for 9.3% thick supercritical airfoil equipped with a single-slotted flap at 30° deflection.

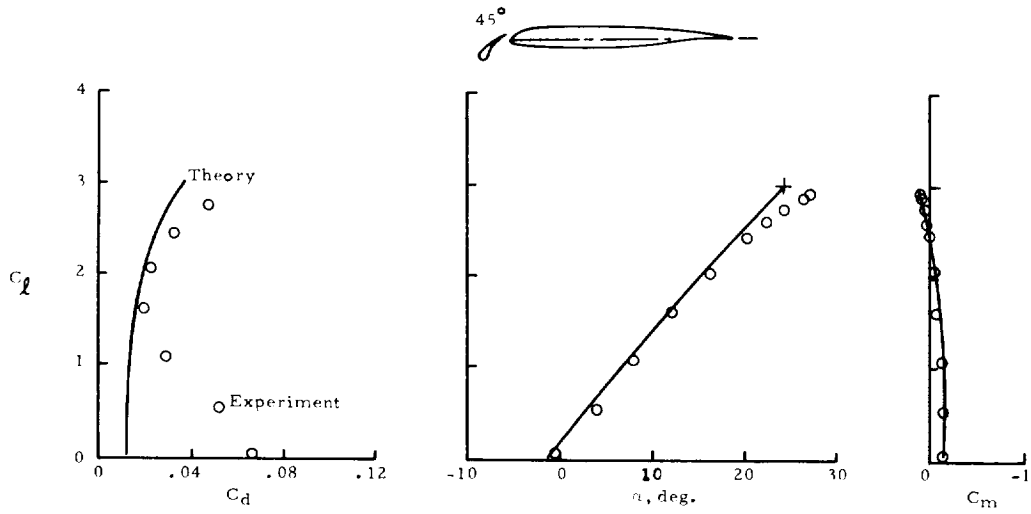

Figure 19.- Theory-experiment comparison for 9.3% thick supercritical airfoil equipped with a leading-edge Krueger.

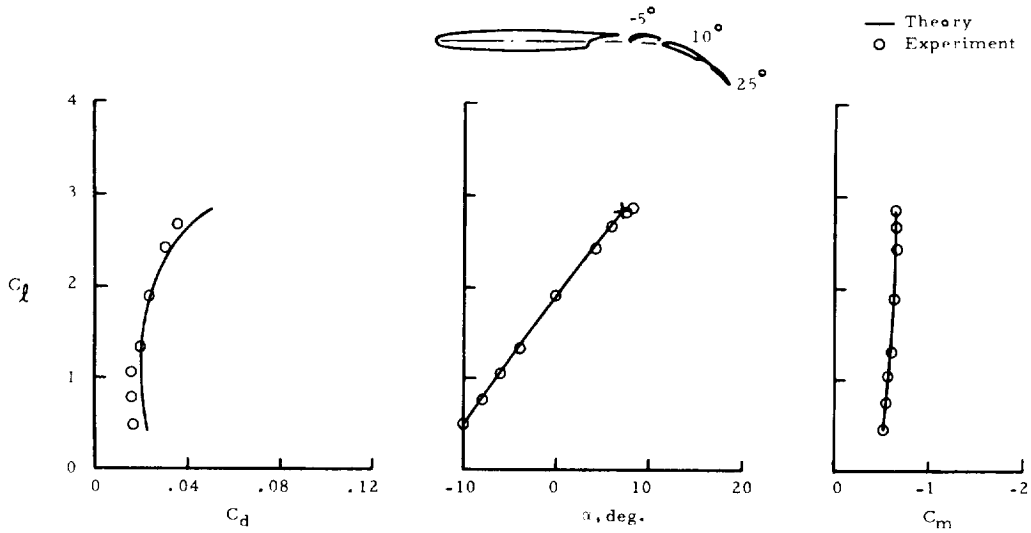

Figure 20.- Theory-experiment comparison for 9.3% thick supercritical airfoil equipped with a triple-slotted flap.

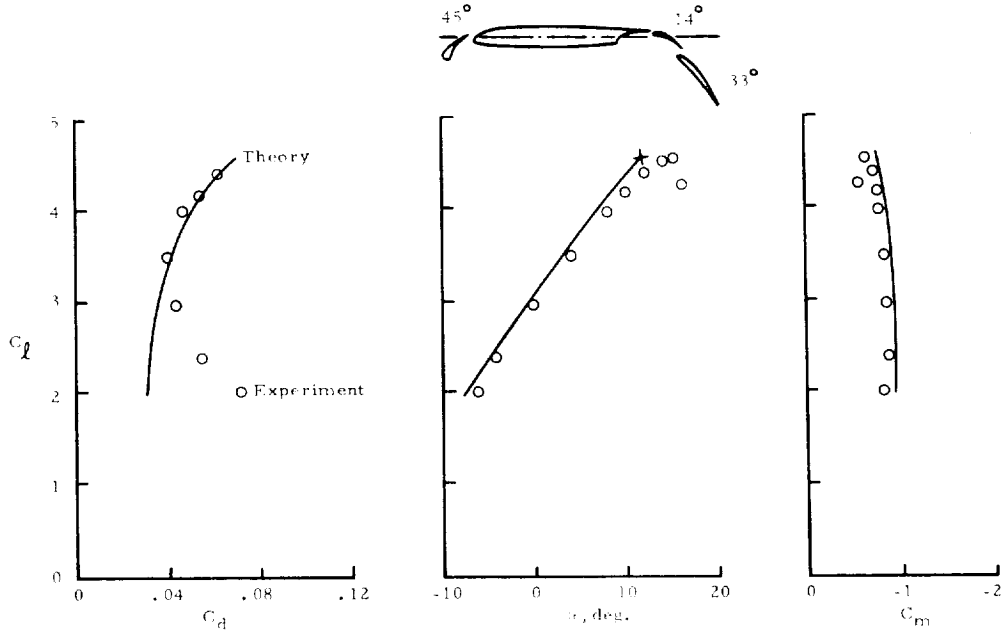

Figure 21.- Theory-experiment comparison for 9.3% thick supercritical airfoil equipped with a leading-edge Krueger and a double-slotted trailing-edge flap.

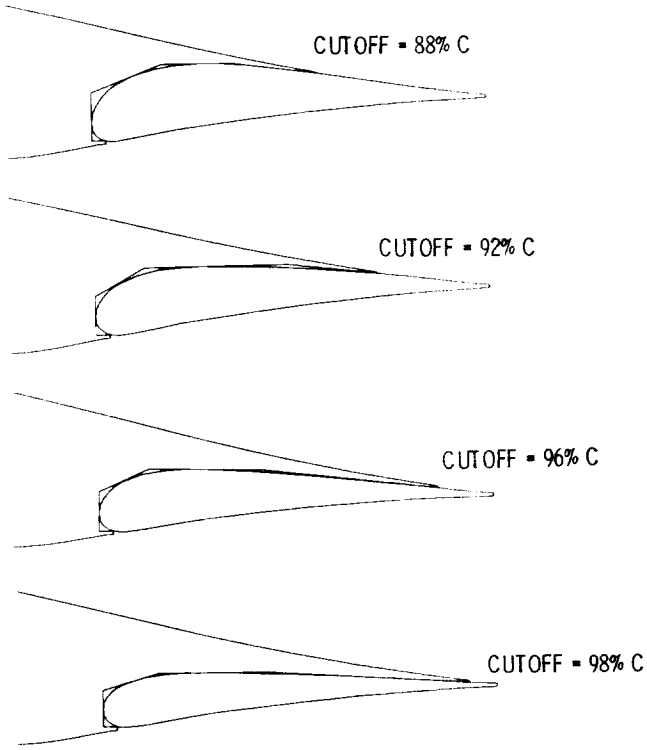

Figure 22.- Single-slotted flap designs for HSNLF(1)-0213 airfoil.

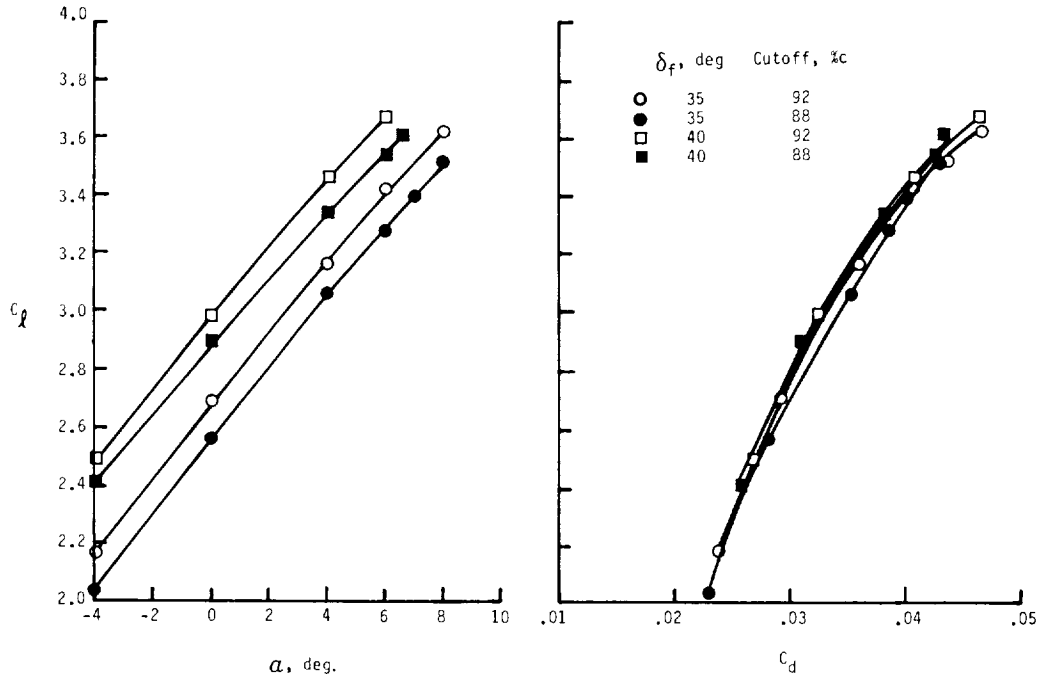

Figure 23.- Effect of 88- and 92-percent chord cutoff on lift and drag coefficient for HSNLF(1)-0213 airfoil. ($R = 4 \times 10^6$)

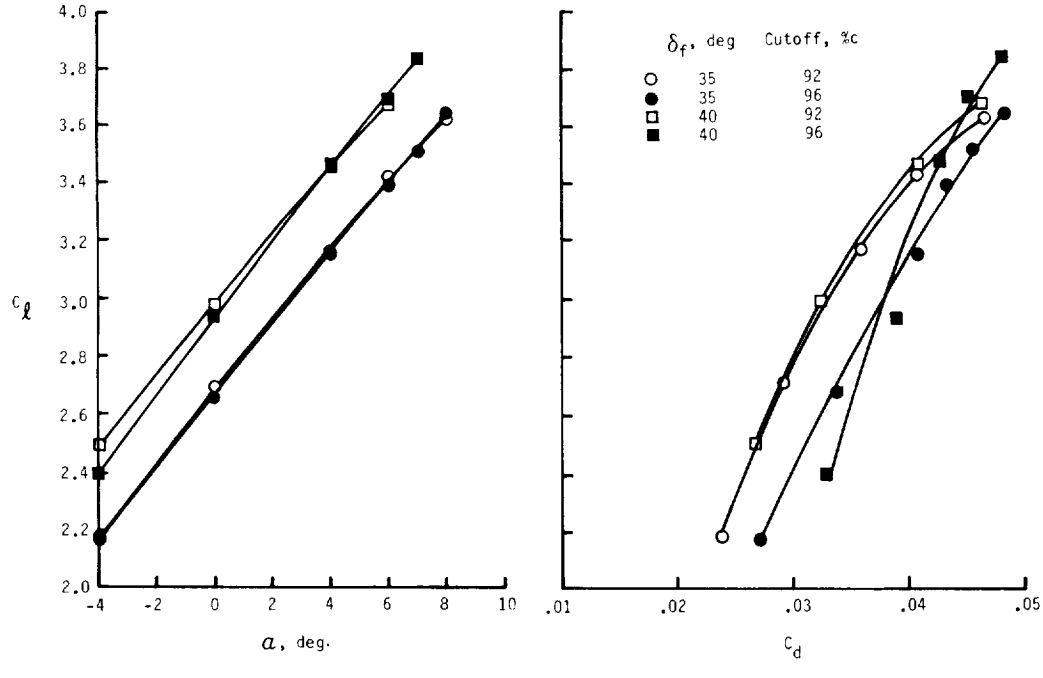

Figure 24.- Effect of 92- and 96-percent chord cutoff on lift and drag coefficient for HSNLF(1)-0213 airfoil. ($R = 4 \times 10^6$)

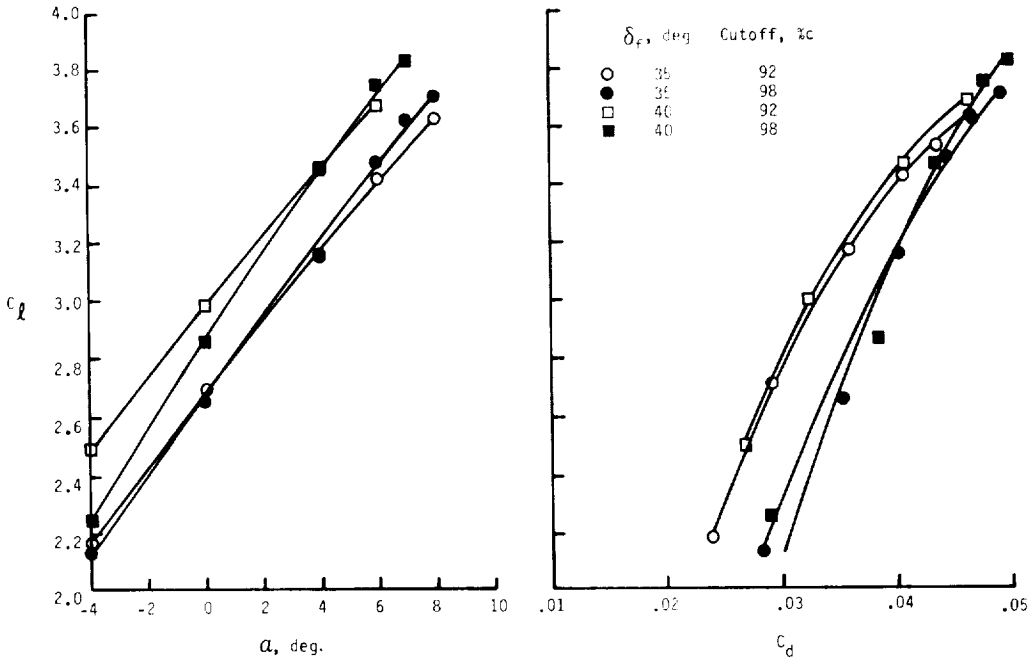

Figure 25.- Effect of 92- and 98-percent chord cutoff on lift and drag coefficient for HSNLF(1)-0213 airfoil. ($R = 4 \times 10^6$)

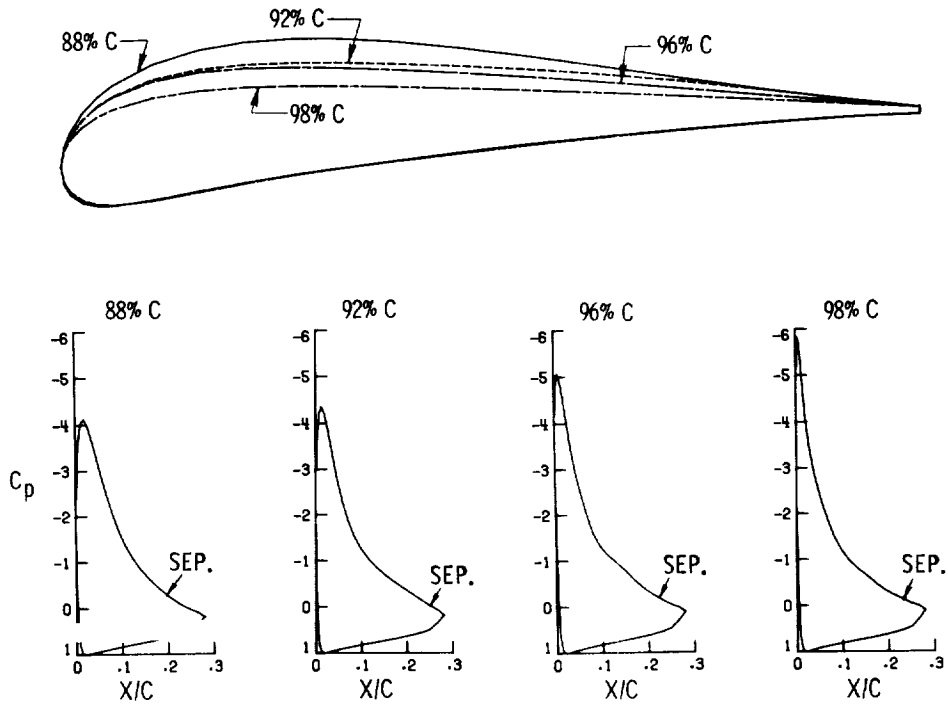

Figure 26.- Geometries and pressure distributions for single-slotted flap designs for HSNLF(1)-0213 airfoil. ($\alpha = 0°$, $R = 4 \times 10^6$, $\delta_f = 35°$)

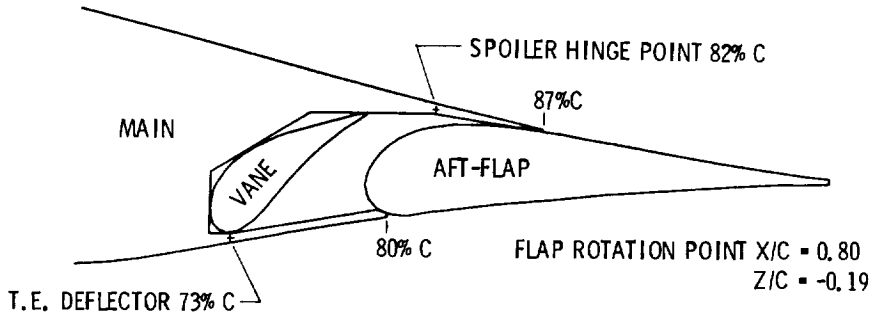

(a) DOUBLE-SLOTTED FLAP

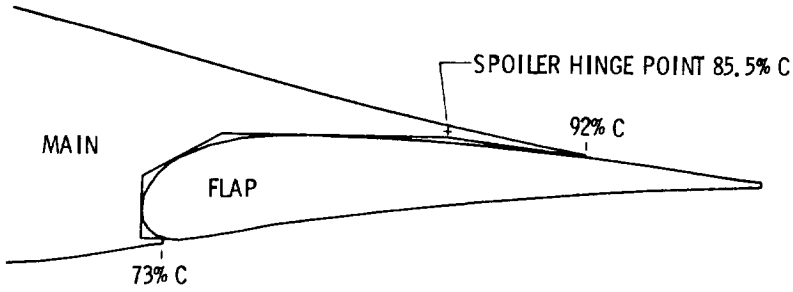

(b) SINGLE-SLOTTED FLAP

Figure 27.- Details of double- and single-slotted flap designs for HSNLF(1)-0213 airfoil.

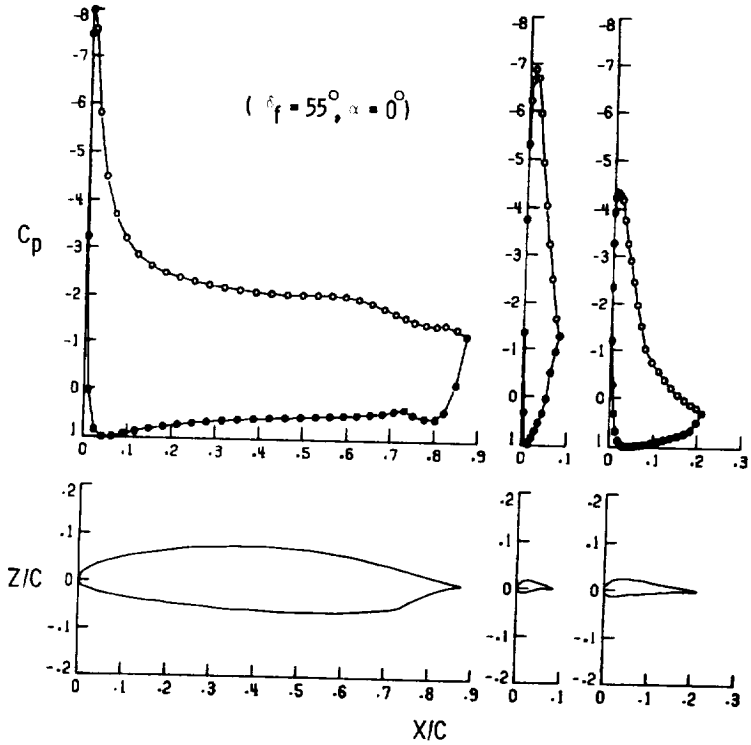

Figure 28.- Sample pressure distribution for HSNLF(1)-0213 airfoil equipped with double-slotted flap. ($R = 4 \times 10^6$)

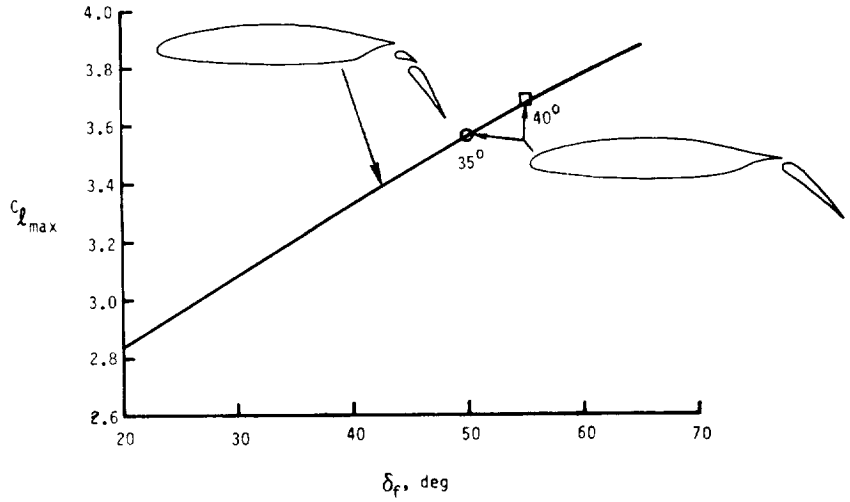

Figure 29.- Effect of flap deflection on maximum lift coefficient for single- and double-slotted flaps. ($R = 4 \times 10^6$)

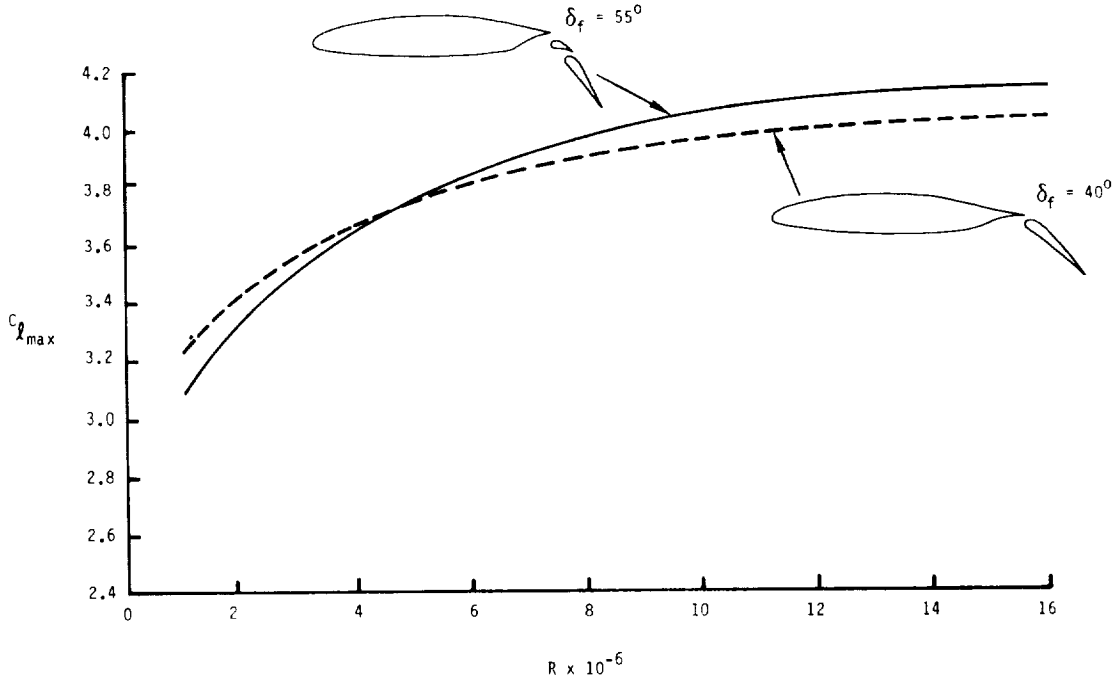

Figure 30.- Effect of Reynolds number on maximum lift coefficient for 55° double-slotted flap and 40° single-slotted flap.

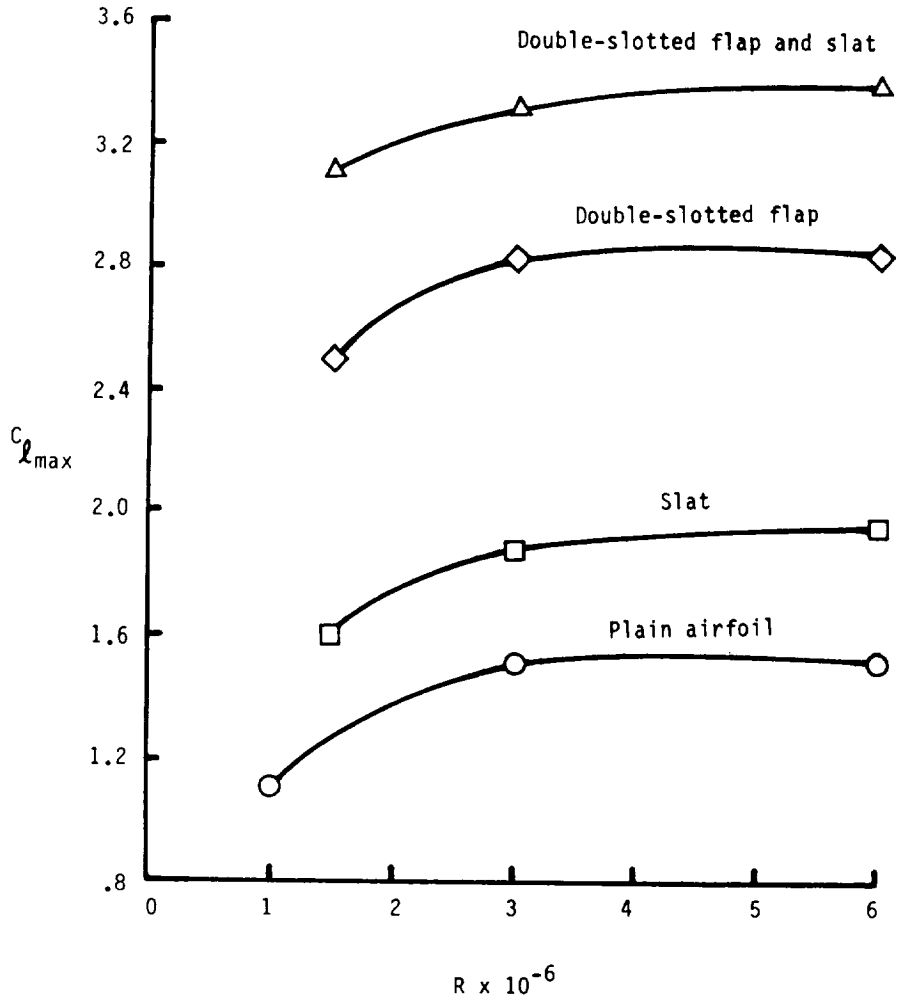

Figure 31.- Effect of slat on maximum lift coefficients for NACA 64_1A212 airfoil with and without double-slotted flap.